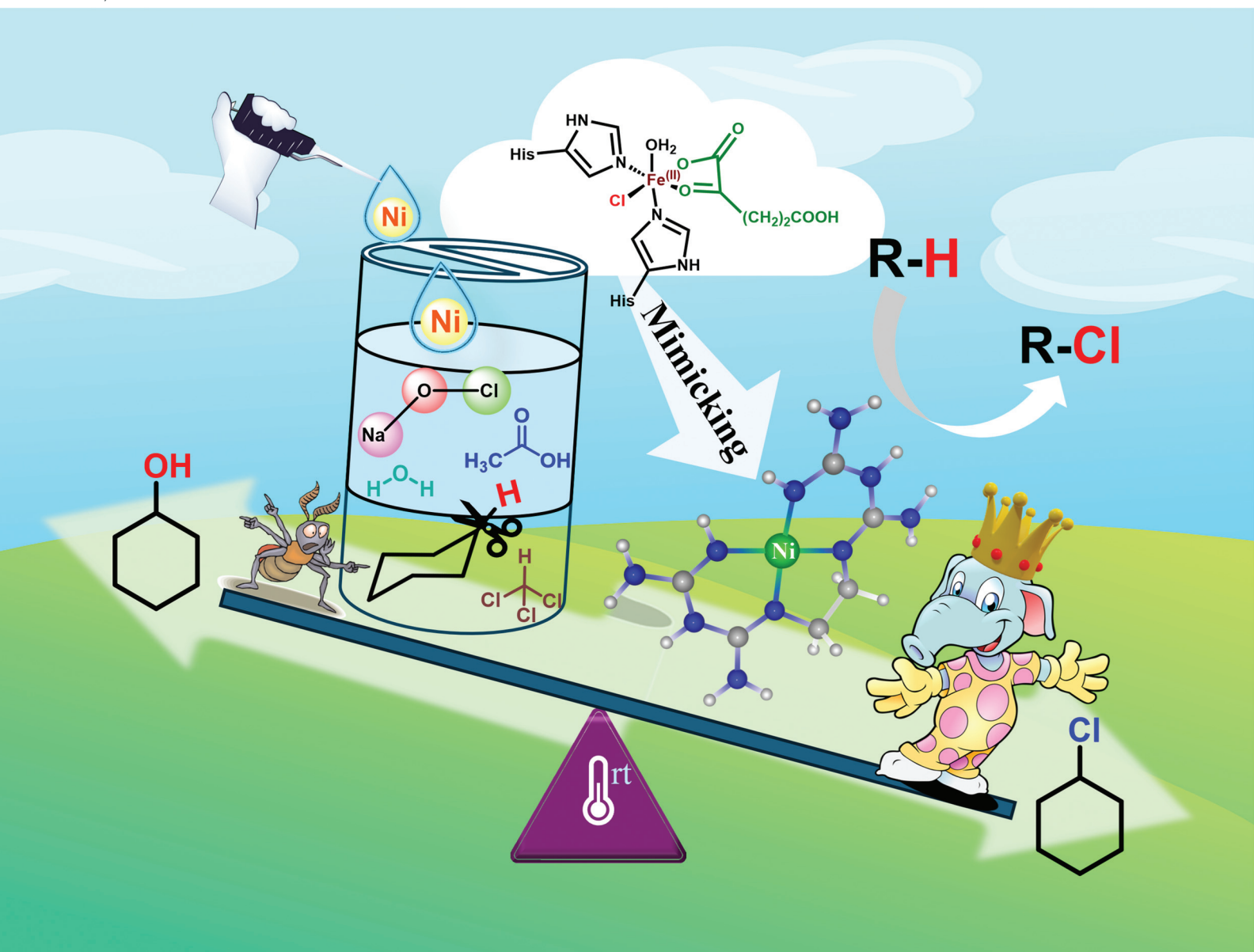


Dalton Transactions

An international journal of inorganic chemistry

rsc.li/dalton



ISSN 1477-9226

PAPER

Basab Bijayi Dhar *et al.*

C-H bond chlorination and bromination using water soluble nickel(II) guanidine complexes

Cite this: *Dalton Trans.*, 2025, **54**, 503

C–H bond chlorination and bromination using water soluble nickel(II) guanidine complexes†

Jaipriya Khatri,^a Vasanthapandiyan Mari,^b Aniruddha Sarkar,^b Nairwit Karmodak^b and Basab Bijayi Dhar^b*^a

Water-soluble nickel(II)-guanidine-based complexes successfully catalyzed the C–H chlorination of a series of hydrocarbons in the presence of NaOCl and acetic acid in water–chloroform (7 : 3, biphasic condition) at room temperature. Majorly chlorinated products (TON ~680 for cyclohexane) were obtained. Furthermore, C–H bond bromination of cyclohexane, *n*-hexane, and toluene was also carried out using *in situ* generation of NaOBr. These putative formations of Ni(III) species were characterized by electron paramagnetic resonance (EPR) spectroscopy, and the plausible mechanism for chlorination was confirmed by DFT calculations.

Received 2nd October 2024,
Accepted 11th November 2024

DOI: 10.1039/d4dt02783c

rsc.li/dalton

Introduction

Catalytic sp³ C–H functionalization is highly demanded in modern industrial and pharmaceutical areas.¹ To date, over 5000 naturally occurring organic halogenated compounds have been identified and characterised.² The incorporation of carbon–halogen bonds in synthetic active pharmaceutical ingredients and natural compounds enhances durability, stability against biodegradation and oxidation, biological activity, and membrane permeability.³ Additionally, over the past four decades, halogenated building blocks have become increasingly important in the development of cross-coupling chemistry (Scheme 1).⁴

In nature, thousands of halogenated molecules are produced exclusively by various metalloenzymes, such as the halogenase SyrB2.⁵ Non-heme iron halogenases are powerful biocatalysts that are capable of halogenating unactivated sp³-hybridized carbon centers with high stereo- and regio-selectivity.^{5c,d} Inspired by the reactivity of the halogenase enzyme, numerous research groups have explored various first-row transition metal complexes to mimic many aspects of this remarkable reactivity toward the activation of inert C–H bonds.⁶ In 2010, Groves and coworkers demonstrated that a highly electron-deficient manganese porphyrin, Mn(TPFPP)Cl, efficiently and

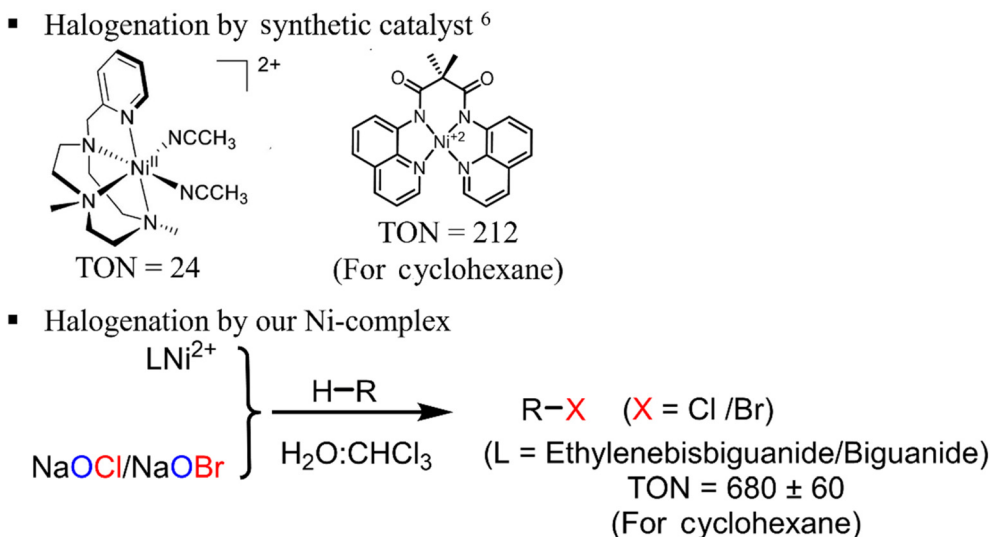
selectively catalyzes C–H chlorination and bromination of various simple alkanes in dichloromethane (DCM) at room temperature (RT).^{6a} Mechanistic studies revealed that the reactive oxomanganese(V) species readily abstracts a hydrogen atom from a substrate C–H bond, forming a substrate-derived radical and an HO–Mn^{IV}(por) intermediate. The HO–Mn^{IV} intermediate then exchanges the hydroxyl ligand with excess hypochlorite anions, which then transfer the chlorine to the alkyl radical. The Costas group used a Ni(II) catalyst with a robust triazacyclononane ligand for the chlorination of alkanes using NaOCl as the terminal oxidant and chloride source.^{6c} Company and coworkers used Ni(II) complexes of a tetradentate macrocyclic bis(amidate) ligand, which showed promising reactivity towards alkanes at –30 °C in the presence of NaOCl.^{6d} In this regard, a terminal Ni(III)–oxygen adduct was characterised by the McDonald research group using a carboxamidate ligand framework.^{6e} Recently, our research group reported that Ni(II) complexes supported by amido-quinoline ligands effectively catalyze C–H chlorination of strong C–H bonds, producing exclusively chlorinated products without any hydroxylated by-products in a mixture of acetonitrile and dichloromethane (8 : 2) at room temperature (RT).^{6f} Despite numerous attempts with various synthetic catalysts using first-row transition metals, a major concern remains the catalyst's solubility and stability in an aqueous medium. Therefore, there is a significant opportunity for synthetic chemists to develop a new catalyst capable of achieving selective halogenation in an aqueous medium.

Guanidines have proven to be powerful N-donor ligands in coordination chemistry and have drawn great attention in the past two decades.⁷ Guanidine is also categorized as an organo-superbase with amine basicity due to the resonance stabilization of its conjugated acids. However, their applications are

^aDepartment of Chemistry, School of Natural Sciences, Shiv Nadar Institution of Eminence Deemed to be University, Delhi NCR, Gautam Buddha Nagar, Dadri, UP-201314, India. E-mail: basabbijayi@gmail.com

^bDepartment of Chemical Sciences, Indian Institute of Science Education and Research Kolkata, Mohanpur 741246, India

† Electronic supplementary information (ESI) available. CCDC 2388373. For ESI and crystallographic data in CIF or other electronic format see DOI: <https://doi.org/10.1039/d4dt02783c>



Scheme 1 C(sp³)-H halogenation by biomimetic Ni(II) guanidine complexes.

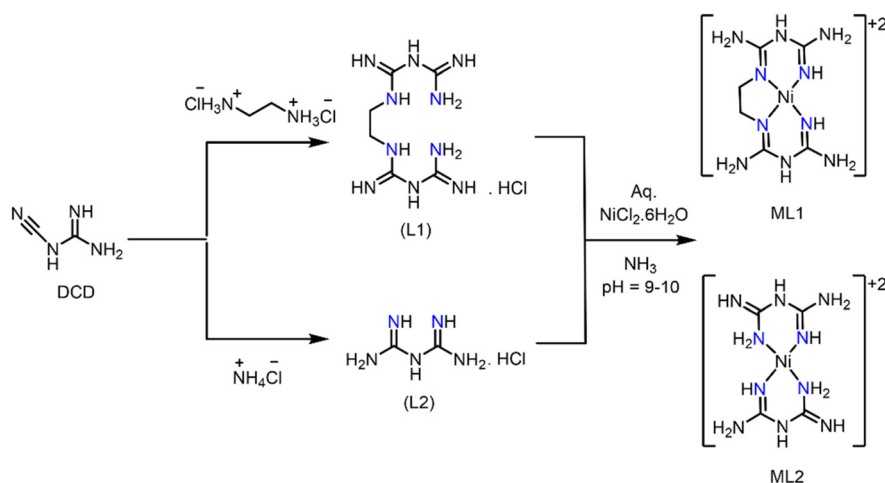
limited to specialized areas such as bioinorganic chemistry,^{7a,b} ionic liquids,^{7c} polymerisation catalysts^{7a} and asymmetric Brønsted-based organocatalysts.^{7a,d} In this report, we highlight that water-soluble guanidine complexes⁸ of Ni(II) successfully chlorinate a series of hydrocarbons (C_{sp³}-H bond energy from 99.3 kcal mol⁻¹ (cyclohexane) to 87 kcal mol⁻¹ (ethylbenzene))⁹ in the presence of NaOCl and acetic acid in a water and chloroform mixture (7 : 3) at room temperature (RT). Furthermore, bromination was carried out by *in situ* generation of NaOBr using an equimolar mixture of NaOCl and NaBr. An insignificant amount of chlorinated product was found with the brominated product.^{6a}

Results and discussion

Characterization of Ni(II) complexes

The nickel(II) complexes were synthesized by the reaction of ammoniacal NiCl₂·2H₂O with ethylenebisbiguanide chloride

(L1) and biguanide chloride (L2) as ligands, respectively (Scheme 2).⁸ The ligands were synthesized according to a reported method with little modification (Fig. S1 and S2†).^{8,10,11} Both complexes were isolated as orange colour crystals and characterized by various analytical techniques. **ML1** exhibits a square-planar geometry with no significant distortion around the nickel center (Fig. 1, Table 1, and Table S1†) as per single-crystal X-ray diffraction data.^{8b,c} The methylene groups were on and out of the plane, and the rings were non-planar. The five-membered ring containing Ni-N1 and Ni-N6 bonds had similar bond lengths, which were larger than the Ni-N3 and Ni-N8 bond lengths. The five-membered chelate angles were smaller than 90°, providing tight chelation around the nickel center. The composition of the Ni(II) guanidine complexes was further confirmed by HR-MS analysis (Fig. S3†). The experimental mass data were matched with the theoretical mass data predicted using Isotope Distribution Calculator (MassHunter software). ¹H and ¹³C NMR spectra of **ML1** and



Scheme 2 Synthetic scheme of Ni(II) guanidine complexes.

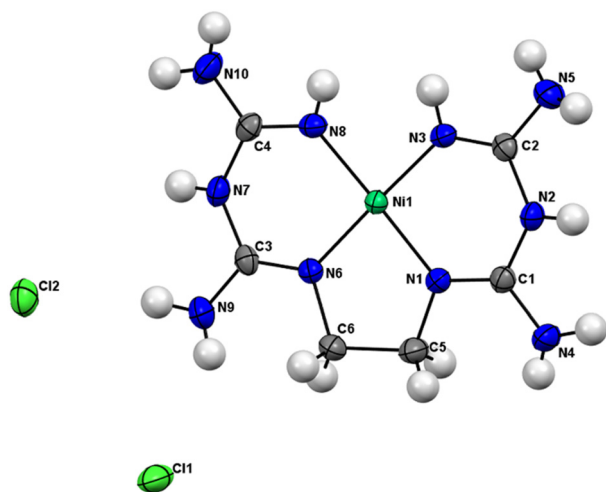


Fig. 1 ORTEP plot of **ML1**. Selective interatomic distances and angles [°] for **ML1**: Ni(1)–N(3) = 1.859 Å, Ni(1)–N(6) = 1.870 Å, Ni(1)–N(1) = 1.870 Å, Ni(1)–N(8) = 1.861 Å, [N(6)–Ni(1)–N(8)] = 92.13°, [N(3)–Ni(1)–N(1)] = 91.98°, [N(3)–Ni(1)–N(8)] = 89.51°, and [N(3)–Ni(1)–N(8)] = 92.13°. The ellipsoids are set at a probability of 50%.

Table 1 Crystal data and structure refinement parameters of the **ML1** complex

Complex	ML1
Empirical formula	C ₆ H ₁₈ Cl ₂ N ₁₀ NiO
Formula weight	375.8906
Temperature (K)	298
Wavelength (Å)	0.71073
Crystal system	Monoclinic
Space group	P ₂ ₁ /n
a (Å)/α (°)	6.90670(10)/90
b (Å)/β (°)	11.6814(2)/100.7390(10)
c (Å)/γ (°)	18.0095(3)/90
Volume (Å ³)	1427.56(4)
Z	4
Density (calc.) (mg m ⁻³)	1.721
Absorption coefficient (μ) (mm ⁻¹)	1.746
F(000)	752
Crystal size (mm ³)	0.221 × 0.204 × 0.184
Theta ranges for data collection	2.008–26.022
Index ranges	–8 ≤ h ≤ 8, –14 ≤ k ≤ 14, –22 ≤ l ≤ 22
Reflections collected	23 837
Independent reflections	2927 [R(int) = 0.0450]
Data/restraints/parameters	2927/0/253
Goodness-of-fit on F ²	1.099
Final R indices	R ₁ = 0.0301
[I > 2σ(I)]	wR ₂ = 0.0312
R indices (all data)	R ₁ = 0.0348
	wR ₂ = 0.0712
Largest diff peak and hole (e Å ⁻³)	0.373 and –0.284

ML2 complexes were examined in order to substantiate the diamagnetic Ni(II) complexes (Fig. S4 and S5†). The CV of the complexes, recorded in methanol, showed a quasi-reversible one-electron wave at $E_{1/2} = 1.11$ V and 1.13 V for **ML1** and **ML2** respectively, using Ag/AgCl (3 M KCl) as a reference electrode at room temperature (RT) (Fig. S6†). The UV-Vis spectra of both the Ni(II) complexes were recorded in water. Both the complexes displayed a similar pattern, with one band in the UV region

around 230–320 nm and a broad band in the visible region around 441–480 nm (Fig. S7†). Frontier molecular orbitals (HOMO and LUMO) obtained from DFT calculations are shown in Fig. S8.† The calculations indicated that the singlet state is the ground state, and the d_{z^2} and $d_{x^2-y^2}$ orbitals correspond to the HOMO and LUMO, respectively.

Reactivity study (chlorination)

The optimization conditions for alkyl chloride formation were performed using **ML1** as the catalyst (0.05 μmol), cyclohexane as the substrate, and NaOCl as both the oxidant and chlorine source in the presence of acetic acid (AcOH) (Fig. S9†). Without AcOH, a black precipitate of NiO was formed, and the yield of the chlorinated product was very low. With 0.30 mmol NaOCl, 0.15 mmol AcOH, and 0.25 mmol cyclohexane in the presence of 0.05 μmol **ML1**, a turnover number (TON) of 680 was achieved within 15 minutes (Table 2, entry 4, Fig. S9,† 22% conversion). The GC and GC-MS chromatograms and NMR spectra indicated the formation of only chlorinated products without any hydroxylated products in the presence of the **ML1** complex (Fig. S10, and S11†). In a control experiment without the nickel complex, a significantly lower product yield (entry 7, ~4.3% compared to **ML1**, entry 4, Table 2) was observed for cyclohexane. An earlier study by the Costas group reported that acetic acid enhances the reaction rate by stabilizing the Ni(III) center.^{6c} Similarly, we found that increasing the acetic acid amount improved the TON (Table 2, entry 4 vs. 5, and Fig. S12†). After optimizing the reaction conditions (Table 2, entry 4, and Fig. S9†), the TON for chlorocyclohexane formation was measured using **ML2** catalysts (Table 2, entry 6, and Fig. S13†). The TON values for **ML1** and **ML2** were significantly higher than those for previously reported Ni(II)-amido quinoline complexes, [Ni^{II}(Pytacn)(CF₃SO₃)₂] (Pytacn = 1-(2-pyridylmethyl)-4,7-dimethyl-1,4,7-triazacyclononane), [Ni^{II}(L)] (L = bis-amidate ligand), and Mn(porphyrin) systems using NaOCl (Table 3, TON varies from 24–212).⁶ Under the optimized conditions (Table 2, entry 4), we investigated the reaction's versatility and applicability across a range of commercially accessible hydrocarbons. The bond dissociation energies of the C(sp³)-H bonds in the substrates varied from 99.3 kcal mol⁻¹ (cyclohexane) to 87 kcal mol⁻¹ (ethylbenzene).⁹ Using toluene as the substrate (Table 4, entry 2, and Fig. S14†), the methyl group

Table 2 Optimization of C–H chlorination^a

Entry	Catalyst	NaOCl (mmol)	TON	Conversion (%)
1	ML1	0.100	250 ± 18	8.10
2	ML1	0.15	373 ± 27	12.1
3	ML1	0.25	552 ± 20	17.9
4	ML1	0.30	680 ± 60	22
5	ML1	0.30 ^b	382 ± 32	12.4
6	ML2	0.30	500 ± 35	16.2
7	—	0.30	—	4.30

^a Reaction conditions (unless otherwise specified): **ML1** (0.05 μmol), substrate (0.25 mmol), NaOCl (0.30 mmol), AcOH (0.15 mmol) in H₂O : CHCl₃ (7 : 3 v/v) 1 mL for 30 min at RT. ^b In the presence of 0.075 mmol AcOH.

Table 3 Catalytic activity of various catalysts for C–H chlorination of cyclohexane with NaOCl in the presence of acetic acid

Entry	Catalyst	Time (h)	Temp. (°C)	TON (chlorination)	Solvent
1	Ni ^{II} L1/NaOCl (this work)	0.5	RT	680 ± 60	H ₂ O : CHCl ₃ (7 : 3)
2	[Ni ^{II} -Amidoquinoline]/NaOCl ^{6f}	0.5	RT	212	ACN : DCM (8 : 2)
3	[Ni ^{III} (L)] (L = bisamidate ligand)/NaOCl ^{6d}	2	-30	44	ACN
4	[Ni ^{II} (Pytacn)(CF ₃ SO ₃) ₂] (Pytacn = 1-(2-pyridylmethyl)-4,7-dimethyl-, 4,7-triazacyclononane)/NaOCl ^{6c}	2	RT	24	ACN
5	Mn(TPP)Cl/NaOCl ^{6a}	2	RT	87	DCM

Table 4 Catalytic C–H chlorination and bromination of cyclic, benzylic, and linear alkanes^a

Entry	Substrate	Product	TON
1			680 ± 60
2			200 ± 20 ^c
3			370 ± 30
4			1600 ± 200(3°); 320 ± 30(2°)
5			260 ± 25
6			130 ± 20
7			108(2°); 27(1°)
8 ^b			125
9 ^b			82
10 ^b			115(2°); 6(1°)

^a Reaction conditions: **ML1** (0.05 μmol), substrate (0.25 mmol), NaOCl (0.30 mmol), AcOH (0.15 mmol) in H₂O : CHCl₃ (7 : 3 v/v) 1 mL for 30 min at RT. ^b **ML1** (0.05 μmol), substrate (0.25 mmol), NaOCl (0.30 mmol), NaBr (0.30 mmol), AcOH (0.15 mmol) in H₂O/CHCl₃ (7 : 3 v/v) 1 mL for 30 min at RT. The products were identified using GC-MS. TON of entries 1–5, 8, and 9 were determined by GC-FID. TON for entry 6 was determined using toluene (25 mmol) as an internal standard. TON of entry 7 was determined by both GC-MS and ¹H-NMR. ^c In complete water medium, TON ~87. Conversion of entries 1–5 is given in Table S2.†

was exclusively halogenated without hydroxylation on the aromatic ring (TON ~200). Chlorination of toluene was also carried in water and product quantification *via* HPLC gave a TON of ~87. In the case of ethylbenzene, 1-chloroethylbenzene was the primary product (TON 370 ± 30 for complex **ML1**), although both secondary and primary C–H bonds were available (Table 4, entry 3, Fig. S15 and S16[†]). For adamantane, the 3°/2° selectivity with **ML1** was 1600 ± 200 and 320 ± 30 , respectively (Table 4, entry 4, Fig. S17 and S18[†]). For 4-methyl biphenyl, the product was 4-(chloromethyl)-1,1'-biphenyl (Table 3, entry 5, Fig. S19 and S20[†]). According to GC-MS analysis, chlorination of 2,3-dimethyl butane occurred at the 3° C–H bond rather than the 1° C–H bond (Table 4, entry 6, and Fig. S21[†]). In the case of *n*-hexane, which has one primary (1° C–H) and two different secondary (2° C–H) bonds with identical bond dissociation energies, the reaction showed ~4 times more chlorination at the 2° C–H bond over the 1° C–H bond (Table 4, entry 7, and Fig. S22[†]). Selectivity for the 2-position was 1.4 times greater than that for the 3-position, as determined by ¹H-NMR (Table 4, entry 7, Fig. S23 and S24[†]). This is likely due to the radical generated at the 2-position being more favourable due to electronic (hyper-conjugation) and steric factors.¹² A similar result was also observed for *n*-pentane (Fig. S25[†]). In Table S4,[†] the reactivity of **ML1** was compared with previously reported first row transition metal complexes.

Reactivity study (bromination)

We extended our chlorination studies to the bromination of benzylic and aliphatic substrates. Instead of NaOBr, a combination of equimolar NaBr and NaOCl was used to generate *in situ* hypobromite (details are given in the ESI[†]).¹³ The bromination of cyclohexane yielded cyclohexyl bromide as the major product (TON ~125) with minimal cyclohexyl chloride (TON ~2), indicating that the hypobromite serves as the halogen source rather than the solvent or the axial ligand (Table 4, entry 8, Fig. S26 and S27[†]). For toluene as a substrate, the TON was found to be 82 with 100% selectivity for benzyl bromide (Table 4, entry 9). Bromination of *n*-hexane was confirmed by GC-MS analysis (Table 4, entry 10, and Fig. S28[†]) and more bromination was observed at the 2° C–H bond.

Mechanistic findings

To gain insight into the mechanism, we performed chlorination reactions for substituted ethylbenzene bearing electron-donating and electron-withdrawing groups. We found that ethylbenzene with an electron-donating group is more prone to oxidation. It implies that the formation of an electrophilic intermediate, which might be stabilized by the electron-donating group in substituted ethylbenzene, could be explained by the negative ρ value (–1.90) obtained from the Hammett plot (Fig. 2a and Fig. S29[†]). After that, various spectroscopic techniques were used to identify the reactive intermediate. On the addition of one equivalent (eq.) of NaOCl and one eq. of AcOH, the light orange solution of the **ML1** complex (1 mM) became darker, and a broadband was observed at 395 nm (Fig. S30 and S31[†]). Extensive HR-MS studies (considering the

dianionic form of ligand **L1**, basic condition) identified the intermediate species such as [Ni(III)-L1-OH] (formula: C₆H₁₅N₁₀ONi, *m/z*: 301.0760, molecular ion peak), [Ni(III)-L1-Cl] (formula: C₆H₁₄N₁₀ClNi, *m/z*: 319.0435, molecular ion peak) and [Ni(III)-L1-OCl] (formula: C₆H₁₄N₁₀ClONi, *m/z*: 335.0350, molecular ion peak) for **ML1** ([**ML1**] = 5 mM) in the presence of 2 eq. NaOCl and 2 eq. AcOH (Fig. S32[†]). However, when considering the monoanionic form of the ligand **L1**, the *m/z*: 301.0760 peak in the HR-MS spectrum could be attributed to [Ni(III)-L1-O]⁺ (formula: C₆H₁₅N₁₀ONi⁺). The EPR spectra of complex **ML1** in the presence of NaOCl (5 eq.) and AcOH (2 eq.) indicated the presence of a single *S* = 1/2 Ni(III) species having *g* values of *g*_x = 2.271, *g*_y = 2.23, and *g*_z = 2.010 (Fig. 2b and Fig. S33[†]).^{6d} Furthermore, the kinetic isotopic effect (KIE) experiment for the chlorination reaction by conducting intermolecular competition experiments with cyclohexane and deuterated cyclohexane (d₁₂) at RT (Scheme S1[†]) was performed for the **ML1** complex. The KIE (*k*_H/*k*_D) value of 12.2 suggests that C–H abstraction is the rate-determining step (RDS) (Fig. S34[†]). The Groves group reported a large kinetic isotopic effect (KIE = 8.7 ± 0.7) for Mn(TPP)Cl, indicating C–H abstraction as the rate-limiting step.^{6a} However, in the absence of **ML1**, the KIE value was found to be only 0.95.

Plausible mechanism

Based on our experimental findings and previous literature, the plausible reaction mechanism is illustrated in Fig. 3. The reaction begins with the oxidation of the metal complex (**ML1**) in the presence of an alkaline NaOCl solution, leading to the formation of a [Ni(III)-O[•]] intermediate. In the next step, [Ni(III)-L-O[•]] abstracts a hydrogen atom (H[•]) from the substrate, forming an alkyl radical and the hydroxo Ni(III) complex, [Ni(III)-L-OH]. To prove this, a reaction was performed in the presence of the radical scavenger TEMPO (2–5 eq.); the TEMPO-alkyl radical adduct was detected by HR-MS, and a significant change in the TON was observed (Fig. S35 and S36[†]). The hydroxide ion on the Ni(III) complex can be substituted by OCl[–] or Cl[–] in the presence of acetic acid, leading to the formation of [Ni(III)-L(OCl)] or [Ni(III)-L(Cl)].^{6a,f} The abstraction of the chlorine radical from the [Ni(III)-L-OCl] complex by the alkyl radical would generate the chlorinated product. Alternatively, *via* Cl rebound from [Ni(III)-L(Cl)], the desired product could also be generated. Additionally, the OH rebound pathway from [Ni(III)-L-OH] could lead to the formation of alkyl hydroxide.^{6c,d} To support this proposed mechanism, we performed density functional theory (DFT) calculations. The reactivity trend and the selectivity between the halogenated *vs.* hydroxylated products were determined following the reaction-free energy calculations and transition state (TS) analysis.

DFT studies. Geometry optimizations were done to figure out the stable spin states of the metal complexes. The most stable spin states of the metal complexes were considered for obtaining the stable structures of the reaction intermediates and reaction-free energy values. The optimized geometries of metal complexes (ML) are shown in Fig. 4. The comparison of the metal–N bond distances of ML_x shows a close resemblance

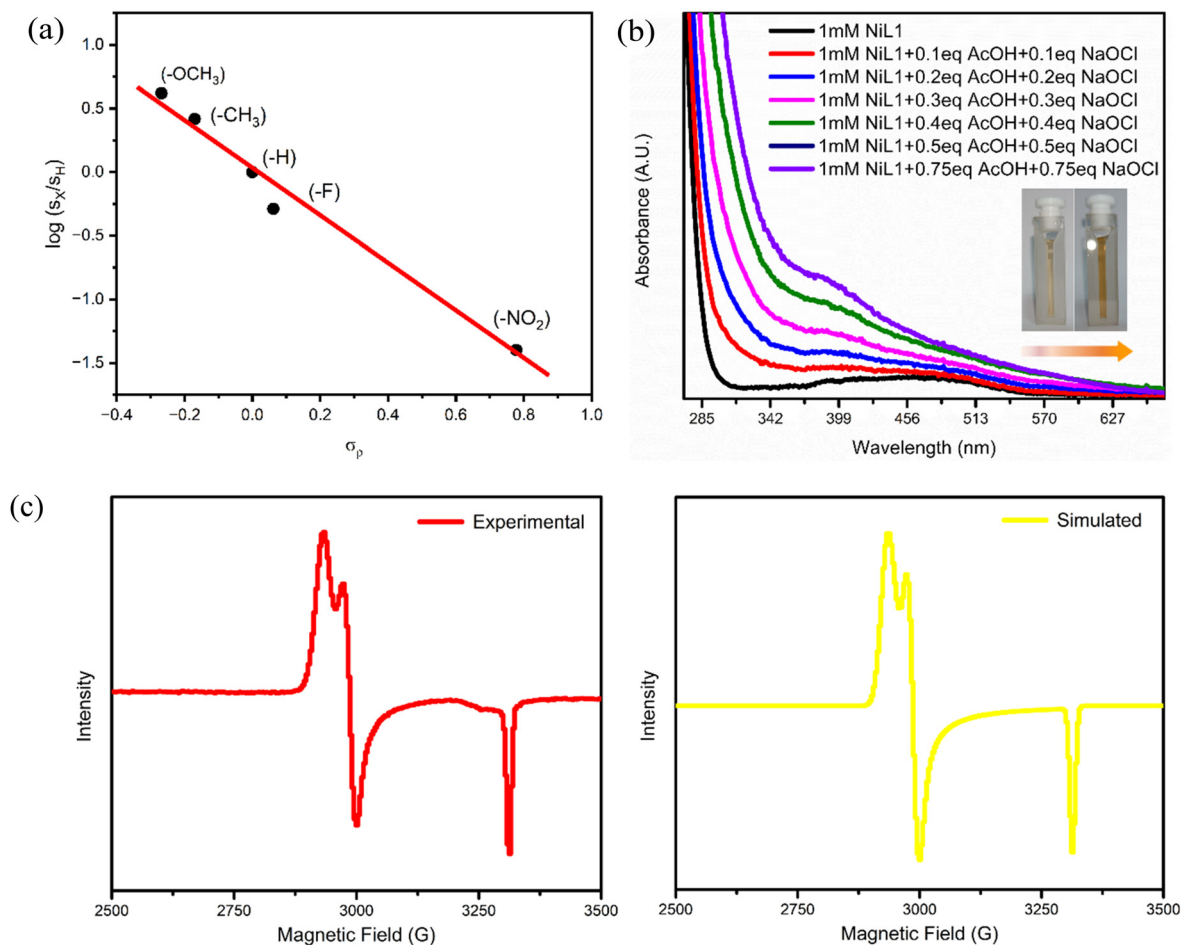


Fig. 2 (a) Hammett plot of chlorination for substituted ethylbenzene with catalyst ML1; (b) UV-Vis spectral change observed after the addition of 1 eq. NaOCl and 1 eq. AcOH in ML1 solution ($[ML1] = 10 \text{ mM}$); (c) EPR spectra of ML1 ($[ML1] = 5 \text{ mM}$) on addition of 2 eq. AcOH and 5 eq. NaOCl. EPR simulation was carried using SimFonia software.

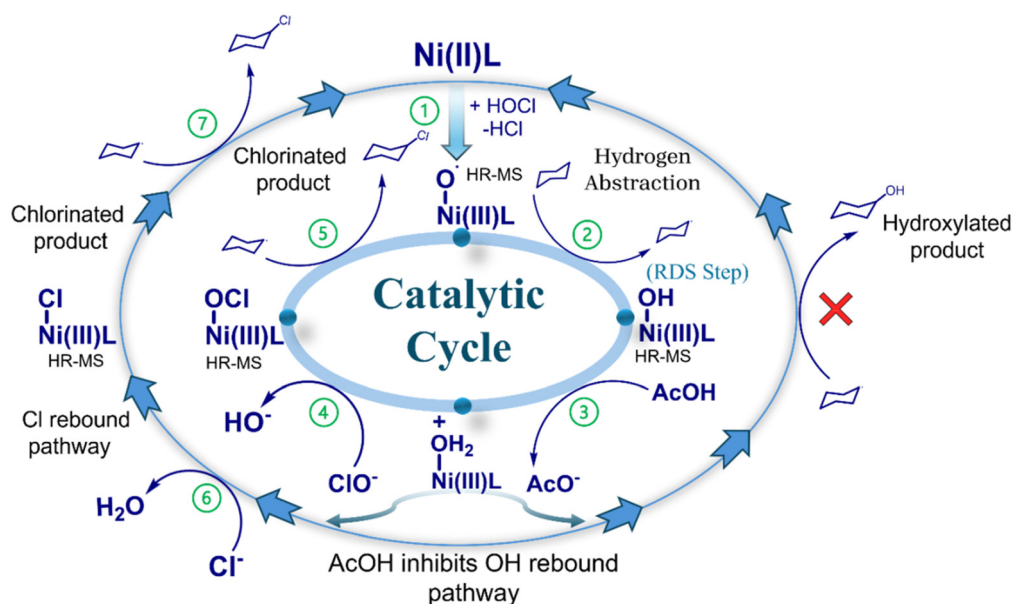


Fig. 3 Proposed mechanism of C-H chlorination.

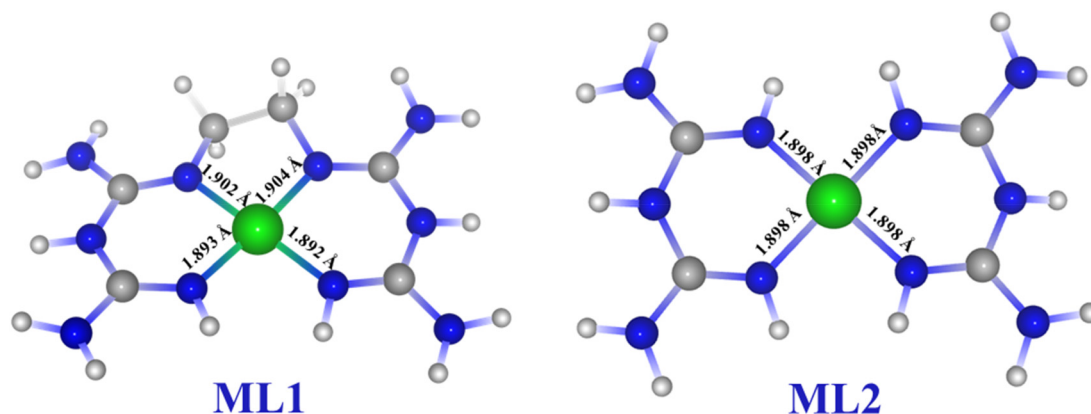


Fig. 4 Optimized DFT structures of the metal complexes (Ni metal in the +2 oxidation state and ground state spin-singlet) are considered in this study (atoms in blue – nitrogen, green – nickel, white – hydrogen).

to the experimental bond distances obtained from the X-ray crystal structure of the complexes (Table S3†).

The reaction-free energies for all the steps were found to be exothermic in nature. Fig. 5a shows the reaction free energy diagram (FED) of the **ML1** complex, while the FED for **ML2** is provided in Fig. S37.† In accordance with the experiment and DFT studies, we identified the proton radical abstraction from the alkyl moiety as the RDS (Fig. 4). We calculated the TS barrier for this step for both the metal complexes, as shown in Fig. 5b. **ML1** had the lowest TS barrier of 11.64 kcal mol⁻¹, whereas **ML2** showed a significantly higher TS barrier of 17.60 kcal mol⁻¹. The TS barriers followed the trend: **ML1** < **ML2**, which correlates with the observed catalytic activity as **ML1** > **ML2**. We performed a Natural Bonding Orbital (NBO) analysis to quantify the spin density of the nickel oxyl [Ni(III)-L-O[•]] intermediate. The observed spin density values of around

~1.55 for both **ML1** and **ML2** confirm their radical nature (Table S4†).

To understand the selectivity between the Cl vs. OH rebound pathway, we performed potential energy scans for the abstraction of both Cl and OH radicals from the **ML1**-OCl/Cl and **ML1**-OH complexes, respectively. The reaction-free energy values were comparable for both pathways, and no TS barrier was observed in either case. However, in the presence of acetic acid, the hydroxylated **ML1** complex (**ML1**-OH) underwent protonation, forming a water-bound intermediate (step 5 in Fig. 3). The transition state barrier for this protonation step was minimal (1.78 kcal mol⁻¹). Following protonation of the hydroxylated complex [Ni(III)-L(OH₂)], the substitution of adsorbed water by OCl⁻ or Cl⁻ ions was highly favourable, with free energies of -31.50 and -37.05 kcal mol⁻¹, respectively. This step favoured the Cl rebound pathway over the OH

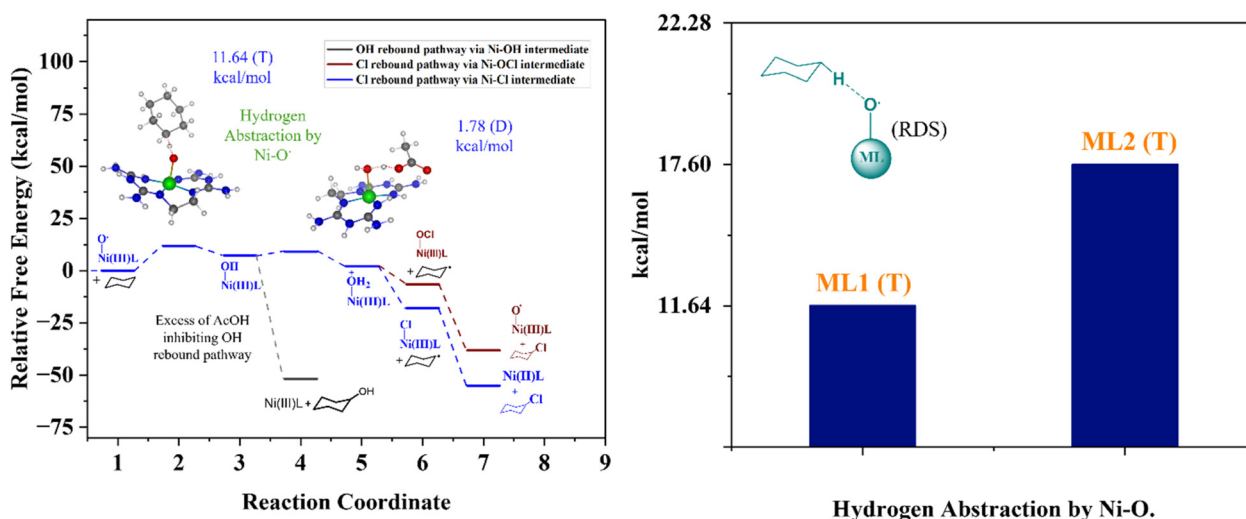


Fig. 5 (a) Free energy diagram for the chlorination and hydroxylation reaction pathways for the **ML1** complex. The transition state geometries are shown. The free energies (in kcal mol⁻¹) were calculated at the M06L/B3LYP functional and 6-311G+(d,p) and in the presence of implicit water as the solvent. (b) Kinetic energy barriers for the HAA by [Ni(III)-L-O[•]]. The transition energy barriers show the following trend: **ML1** < **ML2**.

rebound pathway. Our calculations align with previous studies, where protonation of the hydroxylated Ni(III) complex in the presence of solvated acetic acid was found to disfavour the OH rebound pathway compared to the Cl rebound mechanism.^{6,14}

Conclusion

In summary, we successfully synthesized and investigated two nonheme Ni(II) complexes using guanidine-based ligands. These complexes demonstrated high efficiency in halogenating strong C–H bonds, with bond dissociation energy (BDE) levels ranging from 99.3 kcal mol⁻¹ (cyclohexane; TON ~680) to 87 kcal mol⁻¹ (ethylbenzene; TON ~370). The combination of equimolar NaBr and NaOCl produced majorly brominated products.

Data availability

The data supporting this article have been included as part of the ESI.†

Conflicts of interest

There are no conflicts to declare.

Acknowledgements

BBD acknowledges CSIR, New Delhi (Grant No. EMR-II 80 (0086)/17), for funding. JK and VM acknowledge SNIoE and Shiv Nadar Foundation for the fellowship and computational support (high-performance computing system MAGUS). AS acknowledges CSIR, New Delhi, for the fellowship. NK acknowledges SNIoE for computational support and funding.

References

- (a) R. G. Bergman, *Nature*, 2007, **44**, 391–393; (b) P. Gandeepan, T. Müller, D. Zell, G. Cera, S. Warratz and L. Ackermann, *Chem. Rev.*, 2019, **119**, 2192–2452; (c) U. Dhawa, N. Kaplaneris and L. Ackermann, *Org. Chem. Front.*, 2021, **8**, 4886–4913.
- (a) W.-J. Chung and C. D. Vandewal, *Angew. Chem., Int. Ed.*, 2016, **55**, 4396–4434; (b) C. Crowe, S. Molyneux, S. V. Sharma, Y. Zhang, D. S. Gkotsi, H. Connaris and R. J. M. Goss, *Chem. Soc. Rev.*, 2021, **50**, 9443–9481.
- (a) L. C. Blasiak and C. L. Drennan, *Acc. Chem. Res.*, 2009, **42**, 147–155; (b) C. S. Neumann, D. Galonić Fujimori and C. T. Walsh, *Chem. Biol.*, 2008, **15**, 99–109.
- C. C. C. Johansson Seechurn, M. O. Kitching, T. J. Colacot and V. Snieckus, *Angew. Chem., Int. Ed.*, 2012, **51**, 5062–5085.
- (a) L. C. Blasiak, F. H. Vaillancourt, C. T. Walsh and C. L. Drennan, *Nature*, 2006, **440**, 368–371; (b) F. H. Vaillancourt, J. Yin and C. Walsh, *Proc. Natl. Acad. Sci. U. S. A.*, 2005, **102**, 10111–10116; (c) B. F. Fisher, H. M. Snodgrass, K. A. Jones, M. C. Andorfer and J. C. Lewis, *ACS Cent. Sci.*, 2019, **5**, 1844–1856; (d) T. Hayashi, M. Ligibel, E. Sager, M. Voss, J. Hunziker, K. Schroer, R. Snajdrova and R. Buller, *Angew. Chem., Int. Ed.*, 2019, **58**, 18535–18539.
- (a) W. Liu and J. T. Groves, *Acc. Chem. Res.*, 2015, **48**, 1727–1735; (b) S. Rana, J. P. Biswas, A. Sen, M. Clémancey, G. Blondin, J.-M. Latour, G. Rajaraman and D. Maiti, *Chem. Sci.*, 2018, **9**, 7843–7858; (c) A. Draksharapu, Z. Codolà, L. Gómez, J. Lloret-Fillol, W. R. Browne and M. Costas, *Inorg. Chem.*, 2015, **54**, 10656–10666; (d) T. Corona, A. Draksharapu, S. K. Padamati, I. Gamba, V. Martin-Diaconescu, F. Acuna-Parés, W. R. Browne and A. Company, *J. Am. Chem. Soc.*, 2016, **138**, 12987–12996; (e) P. Pirovano, E. R. Farquhar, M. Swart and A. R. McDonald, *J. Am. Chem. Soc.*, 2016, **138**, 14362–14370; (f) S. Adhikari, A. Sarkar and B. B. Dhar, *Chem. Commun.*, 2022, **58**, 4075–4078; (g) K. Yu, K. Zhang, T. Jakob, R. P. Maier and T. R. Ward, *Chem. Commun.*, 2024, **60**, 1944–1947.
- (a) X. Cui, C.-H. Tan and D. Leow, *Org. Biomol. Chem.*, 2019, **17**, 4689–4699; (b) C. Alonso-Moreno, A. Antinolo, F. Carrillo-Hermosilla and A. Otero, *Chem. Soc. Rev.*, 2014, **43**, 3406–3425; (c) J. Shah, H. Blumenthal, Z. Yacob and J. Liebscher, *Adv. Synth. Catal.*, 2008, **350**, 1267–1270; (d) D. Leow and C.-H. Tan, *Chem. – Asian J.*, 2009, **4**, 488–507.
- (a) P. Ray, *Chem. Rev.*, 1961, **61**, 313–359; (b) B. L. Holian and R. E. Marsh, *Acta Crystallogr., Sect. B*, 1970, **26**, 1049–1058; (c) T. C. Creitz, R. Gsell and D. L. Wampler, *J. Chem. Soc. D*, 1969, **23**, 1371–1372.
- M. Ghosh, K. K. Singh, C. Panda, A. Weitz, M. P. Hendrich, T. J. Collins, B. B. Dhar and S. S. Gupta, *J. Am. Chem. Soc.*, 2014, **136**, 9524–9527.
- D. Karipides, W. C. Fernelius and M. D. Joeston, *Inorg. Synth.*, 2007, **7**, 55–58.
- E. Dittler, *Monatsh. Chem.*, 1908, **29**, 645–652.
- H. Hu, Y. Su, X. Cui, B. Zhao, J. Chen, S. Chen, M. Chen, H. Huo and C. Wang, *Cell Rep. Phys. Sci.*, 2023, **4**, 101362.
- S. Sathyamoorthi, S. Banerjee, J. Du Bois, N. Z. Burns and R. N. Zare, *Chem. Sci.*, 2017, **9**, 100–104.
- (a) S. Pandian, M. A. Vincent, I. H. Hillier and N. A. Burton, *Dalton Trans.*, 2009, **31**, 6201–6207; (b) H. Noack and P. E. M. Siegbahn, *J. Biol. Inorg. Chem.*, 2007, **12**, 1151–1162; (c) H. M. Senn, *Front. Chem.*, 2014, **2**(15), 1–12; (d) A. Timmins and S. P. De Visser, *Catalysts*, 2018, **8**, 314.